

Article

Oxidation and Ablation Behavior of Particle-Filled SiCN Precursor Coatings for Thin-Film Sensors

Lanlan Li ^{1,2}, Yingping He ^{1,2}, Lida Xu ^{1,2}, Chenhe Shao ^{1,2}, Gonghan He ^{1,2}, Daoheng Sun ^{1,*} and Zhenyin Hai ^{2,*}

¹ Department of Mechanical and Electrical Engineering, School of Aerospace Engineering, Xiamen University, Xiamen 361102, China; lilanlan1006@163.com (L.L.); hyp19980504@163.com (Y.H.); superldxu@gmail.com (L.X.); chenhe2019@stu.xmu.edu.cn (C.S.); hgh@xmu.edu.cn (G.H.)

² Fujian Micro/Nano Manufacturing Engineering Technology Research Center, Xiamen University, Xiamen 361102, China

* Correspondence: sundh@xmu.edu.cn (D.S.); haizhenyin@xmu.edu.cn (Z.H.)

Abstract: Polymer-derived ceramic (PDC) thin-film sensors have a very high potential for extreme environments. However, the erosion caused by high-temperature airflow at the hot-end poses a significant challenge to the stability of PDC thin-film sensors. Here, we fabricate a thin-film coating by PDC/TiB₂/B composite ceramic material, which can be used to enhance the oxidation resistance and ablation resistance of the sensors. Due to the formation of a dense oxide layer on the surface of the thin-film coating in a high-temperature air environment, it effectively prevents the ingress of oxygen as a pivotal barrier. The coating exhibits an exceptionally thin oxide layer thickness of merely 8 μm, while its oxidation resistance was rigorously assessed under air exposure at 800 °C, proving its enduring protection for a minimum duration of 10 h. Additionally, during ablation testing using a flame gun that can generate temperatures of up to 1000 °C, the linear ablation rate of thin-film coating is merely 1.04 μm/min. Our analysis reveals that the volatilization of B₂O₃ occurs while new SiO₂ is formed on the thin-film coating surface. This phenomenon leads to the absorption of heat, thereby enhancing the ablative resistance performance of the thin-film sensor. The results indicate that the thin-film sensor exhibits exceptional resistance to oxidation and ablation when protected by the coating, which has great potential for aerospace applications.

Keywords: polymer-derived ceramics; thin-film coatings; oxidation; ablation



Citation: Li, L.; He, Y.; Xu, L.; Shao, C.; He, G.; Sun, D.; Hai, Z. Oxidation and Ablation Behavior of Particle-Filled SiCN Precursor Coatings for Thin-Film Sensors.

Polymers **2023**, *15*, 3319. <https://doi.org/10.3390/polym15153319>

Academic Editor: Marcelo Antunes

Received: 3 July 2023

Revised: 4 August 2023

Accepted: 5 August 2023

Published: 7 August 2023



Copyright: © 2023 by the authors. Licensee MDPI, Basel, Switzerland. This article is an open access article distributed under the terms and conditions of the Creative Commons Attribution (CC BY) license (<https://creativecommons.org/licenses/by/4.0/>).

1. Introduction

The growing demand for monitoring operations in harsh environments has stimulated the advancement of high-temperature sensors. High-temperature thin-film sensors offer significant potential for integration into high-temperature components owing to their advantageous attributes, including micrometer-scale thickness, negligible mass, non-intrusive nature, and minimal interference with surface airflow and component vibration modes [1–3]. Compared with metal materials, the precursors of PDC are generally liquid polymers, and the liquid precursors forming-curing-crosslinking-pyrolysis to form a ceramic structure. Its working ability in extreme environments, such as oxidation resistance and thermal shock resistance, is significantly better than alloys. Polymer-derived ceramics (PDCs), due to their excellent resistance to oxidation and high temperature properties [4], are widely used in high-temperature bulk [5–7] and thin-film sensors. PDC thin-film sensors [8] can be fabricated by an in situ direct writing method, which has a great advantage in the high-temperature sensor field.

Currently, a significant amount of research is focused on exploring the performance of PDC thin-film sensors, including strain gauges [8,9], temperature sensors [10–12], and heat flux sensors [13]. Cui [14] developed a temperature-sensitive sensor using a SiCN film that was less than 100 μm thickness, with a maximum measurement temperature of 800 °C. Wu et al. [9] fabricated TiB₂/SiCN thin-film strain gauges, which can work close

to 800 °C. While most of these fabricated films exhibit stable operation at temperatures ranging from 25 °C to 800 °C, their long-term stability without peeling or oxidation in real high-temperature operating environments is crucial. Therefore, it is crucial to develop an anti-oxidation and anti-ablation thin-film coating for thin-film sensors. Cui et al. [15] successfully prepared a PDC antioxidant coating that can be applied to thin-film sensors up to 800 °C. Xu et al. [16] developed a double-layer high-temperature antioxidant PDC composite film by direct writing. Wu et al. [17] improved the high-temperature stability of SiCN thin-film resistive grids by fabricating Al₂O₃/SiCN composite films. These studies, however, did not investigate the oxidation resistance of the films in depth. Since the PDC composite film is used as an antioxidant layer, it also needs to have resistance to the effect of high-temperature airflow in harsh environments [18,19]. However, their investigation only made a preliminary investigation of the antioxidant properties of the film without studying the ablation resistance of the film.

Although there have been a large number of studies on the ablation resistance of coatings [20–24], Yanjiang et al. [20] prepared TZSS coatings encapsulating C/C substrates with a size of 10 mm × 5 mm × 10 mm, which can be ablated at 4.2 MW/m² for 40 s. Jing'an Kong et al. [21] prepared TaC coatings and performed cyclic oxyacetylene flame tests with a coating thickness of 600 μm. However, these coatings were prepared on C/C substrates with thickened thicknesses. Unlike the bulk coating, the thin-film coating is fabricated in situ on top of the alumina substrate or on top of the thin-film thermistor with a coating thickness in the micron range. The ablation resistance studies of coatings have predominantly concentrated on C/C composites. Unlike these coatings, thin-film coatings are fabricated in situ on substrates or thin-film sensors with specimen thicknesses at the micron level [15,17]. Meanwhile, the investigation into the ablation resistance of thin-film coatings has been limited. Nonetheless, it is crucial to carry out comprehensive studies on the coupling behavior between film oxidation and ablation for practical applications.

In this work, through our analysis of the oxidation and ablation behavior of PDC TiB₂/B composites, we observed that the formation of SiO₂-B₂O₃ on the coating surface is vital for improving the oxidation and ablation resistance of the thin-film sensors. The SiO₂-B₂O₃ oxide layer formed at high temperature is 7~8 μm thick and its well prevented the entry of oxygen. Furthermore, we characterized the ablation process of the film using a butane flame at 1000 °C with a linear ablation rate of 1.04 μm/min. During the ablation process, the B₂O₃ formed on its surface volatilized, and the SiCN thermally decomposed to generate new SiO₂, which absorbed the energy of ablation and played a key role in protecting the sensitive layer of the thin-film sensor. And it was observed that the thin-film sensor maintained a resistance change of 0.075%/min of exposure to the flame spraying test. The results demonstrate that the PDC/TiB₂/B composite thin-film coating enhances the oxidation and ablation resistance of thin-film sensors at high temperatures, making it an option for protective coatings in demanding environments, such as aerospace applications.

2. Experimental Section

2.1. The Fabrication of Thin-Film Coatings

In this study, PSN2 (commercially provided by the Institute of Chemistry, Chinese Academy of Sciences, Beijing, China) was used as the precursor of SiCN. TiB₂ and B powders were used as the filler particles with an average diameter of 1 μm (Shanghai Chaowei Nano Technology Co., Shanghai, China). And there was an alumina base (15 mm × 15 mm × 1 mm) that was used for oxidation and ablation performance tests.

As shown in Figure 1, the preparation process of the coating is described. First, PSN2, B and TiB₂ are mixed according to the mass ratio of 1:0.8:1 to prepare a mixed solution. The PDC composite ink is put on the magneton mixer and stirred at room temperature for 2 h. Next, using the microscale Wie-senberg platform, the mixed ink is written directly onto the alumina substrate. After the direct writing is complete, it is placed on a heated platform and cured at 100 °C for 10 min. Finally, the film is annealed in the air at 800 °C in the muffle

furnace and cooled with the furnace; it reaches the indoor temperature, and can be taken out. The thin-film coating is thus obtained.

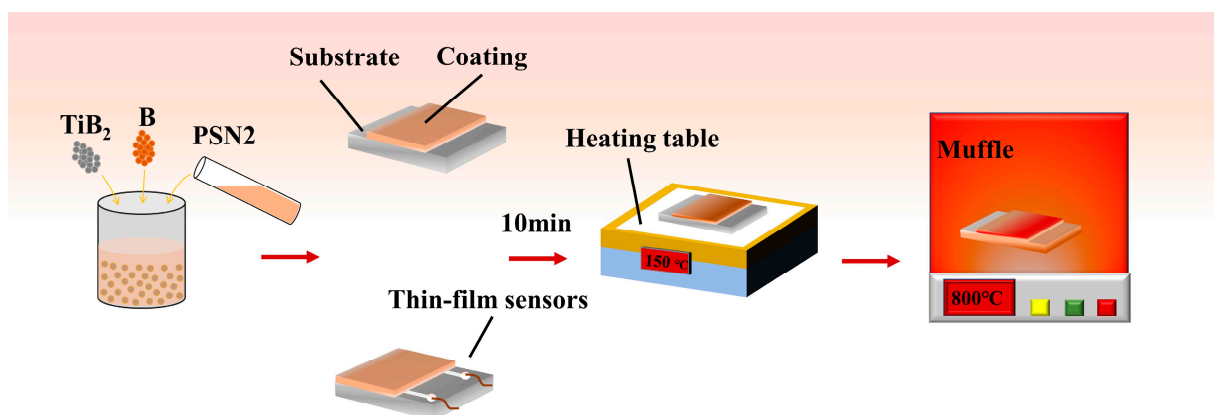


Figure 1. Fabrication process of the coating.

Currently, we are applying the prepared thin-film above the thin-film sensor. By coating the thin-film on the alumina substrate where the sensitive gate is fabricated, Please delete it. The correct statement should be: we can obtain a double-layer thin-film sensor [14]. The resistance of this sensor is characterized by cycling stability at room temperature to 800 °C [14].

2.2. Protection Performance Tests of the Thin-Film Coatings

The furnace was set to 800 °C to test the oxidation resistance of the coating. A thermogravimetric analyzer (TG-DSC, TGA/DSC, STA449F5) was used for the analysis of TiB_2 , B and thin-films. At 800 °C, the oxidation characteristic time was heated at a rate of 10 K/min. The following equation calculated cumulative mass change percentages ($\Delta\text{mass}\%$) of the powders:

$$\Delta\text{mass}\% = \frac{m_t - m_0}{m_0}$$

where m_0 and m_t are the mass of the powder before and after oxidation for t minutes. The curves of mass change with oxidation time were given according to the above calculation formula.

To assess the ablation resistance of the film, a simplified film ablation system was established (Figure 2). The system utilized a flame gun powered by a 95% butane gas stream, with a test temperature of 1000 °C. The flame gun nozzle had an inner diameter of 20 mm and was positioned 6 cm away from the sample. The butane gas flow rate was set at 0.03 L/s. A thermocouple was centrally placed on the sample to monitor the real-time temperature. The film underwent continuous ablation in the flame for durations of 4 min, 10 min, 15 min, and 30 min, and the linear ablation rate was subsequently calculated. The line ablation rate was used to evaluate the ablation resistance.

$$R_m = \frac{\Delta m}{t}$$

where R_m is the line ablation rate, Δm is the coating thickness change, and t is the ablation time.

2.3. Characterization

The sensors were primarily characterized using a profilometer (Dektak XT) to measure their thickness, and scanning electron microscopy with energy-dispersive spectroscopy (SEM-EDS) using a JSM-IT500A instrument from JEOL in Tokyo, Japan, to analyze their morphology and elemental composition. X-ray diffraction (XRD) analysis was performed

using a Shimadzu XRD-6100 instrument. The output resistance of the thin-film sensors was measured using a Keysight 34972A data acquisition device (DAQ).

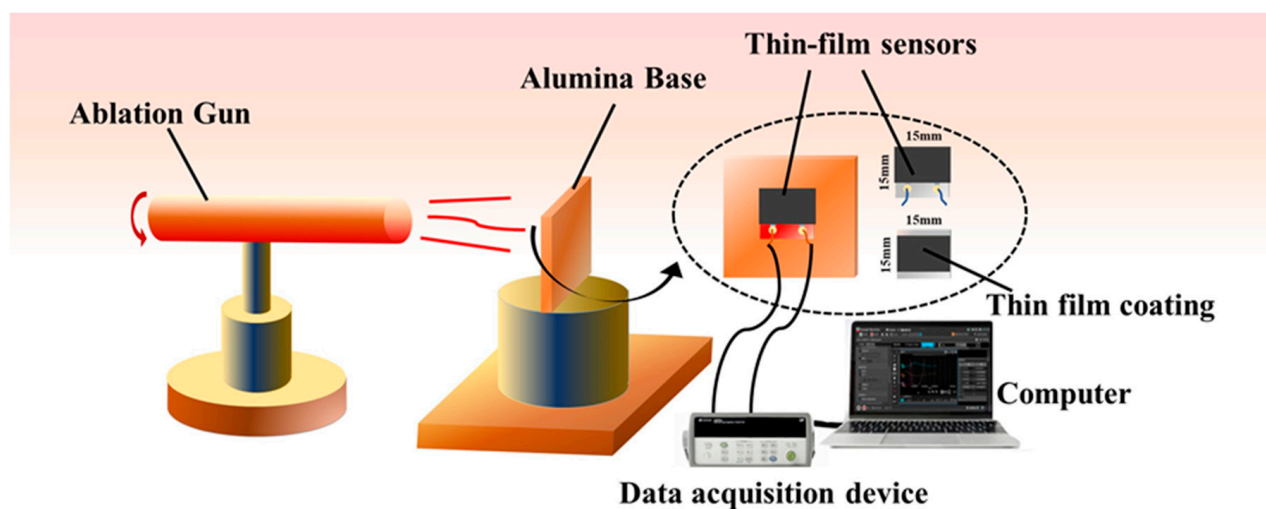


Figure 2. Simple system for film ablation resistance.

3. Results and Discussion

3.1. Phase Analysis and Microstructure of the Thin-Film Coatings

Figure 3a shows the XRD pattern of the prefabricated coating; the TiB_2 phases are detected. Figure 3b,c depict scanning electron microscope (SEM) images of the prefabricated coating surface, providing insight into the distribution and morphology of the raw material particles. The surface exhibits a relatively rough texture and contains noticeable particulate features. EDS analysis of spot 1 (Figure 3c) reveals the presence of titanium (Ti) and boron (B) on the surface. Furthermore, Figure 3(c1) exhibits a uniform distribution of oxygen (O) and silicon (Si) elements, indicating the effective bonding role of PSN2 during the coating fabrication process. Consequently, the surface particles primarily consist of TiB_2 and B. Figure 3d displays a cross-sectional view of the prefabricated coating, showcasing a uniform thickness of approximately $30\ \mu\text{m}$ applied to the alumina surface. The Energy Dispersive Spectrometer (EDS) analysis (Figure 3(d1)) clearly distinguishes titanium (Ti) elements and reveals relatively even distribution of silicon (Si) and aluminum (Al) elements, where Al is the element of the base (Al_2O_3). Notably, no instances of delamination or peeling are observed, except for a few larger TiB_2 particles measuring $1\ \mu\text{m}$. The coating is successfully obtained at room temperature and exhibits excellent adhesion to the alumina substrate.

3.2. Oxidation Behavior of the Thin-Film Coatings

To evaluate the oxidation resistance of the coating, we obtained an isothermal curve by subjecting the coated material to a temperature of $800\ ^\circ\text{C}$ for 12h and air flow of $50\ \text{mL}/\text{min}$ (Figure 4). The curve exhibits three distinct stages: a rapid mass increase (Stage I), a slower mass increase (Stage II), and a plateau (Stage III). After 80 min of oxidation of the coating, its mass increased sharply, reaching $0.15\ \text{wt}\%$. According to the TG-DSC and isothermal oxidation curves (Figure 5a,b) of B powder and TiB_2 powder, the furnace is heated up to $800\ ^\circ\text{C}$ with a rate of $10\ ^\circ\text{C}/\text{min}$, and keeping for $50\ \text{mL}/\text{min}$ of the air flow. It can be seen that there is a large amount of oxygen diffusion in the powder, oxidizing TiB_2 and B particles, producing TiO_2 and B_2O_3 (Figure 5c,d). Based on the literature of the antioxidant thin-film coating, it is required to have a good coefficient of thermal expansion with the substrate and sensitive layers [25,26]. The average alumina substrate thermal expansion coefficient [27] is measured at $7.1 \times 10^{-6}/\text{K}^{-1}$. Additionally, the average thermal expansion coefficients of B and TiB_2 are $6.4 \times 10^{-6}/\text{K}^{-1}$ and $7.0 \times 10^{-6}/\text{K}^{-1}$, respectively [28,29]. Notably, TiB_2 is a well-established high-temperature material that has been successfully utilized in high-temperature thin-film applications [9,30]. Consequently, the combination

of B/TiB₂ offers significant advantages over using only B as the filler, as it achieves a superior thermal match with both the substrate and the sensitive layer of the thin-film sensor. This enhanced thermal match ensures improved overall performance and stability for the thin-film sensor. As oxidation time increases, mass gain enters a slow phase (II stage). The mass plateau stage is in III stage with a mass gain of 0.2 wt%.

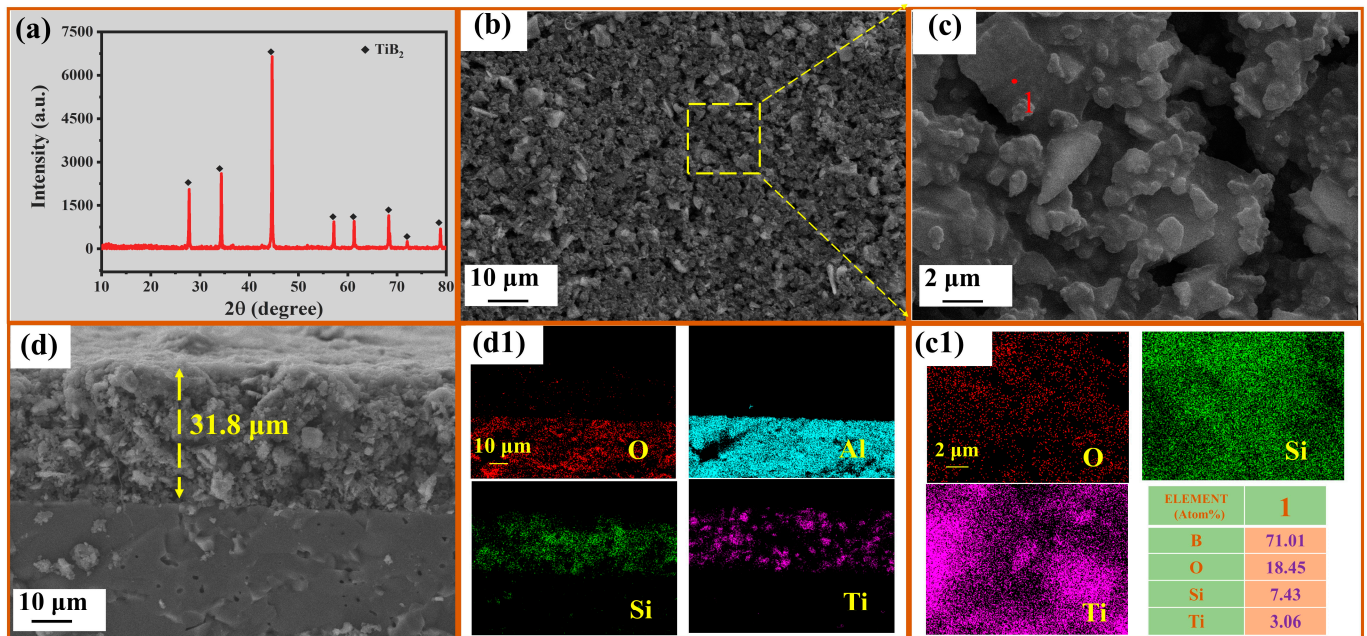


Figure 3. (a) XRD pattern of the surface; (b) Surface image of the prefabricated coating; (c) local surface of (a); (c1) EDS analysis of (c) and spot 1; (d) cross-sectional image of the coating; (d1) EDS analysis of (d).

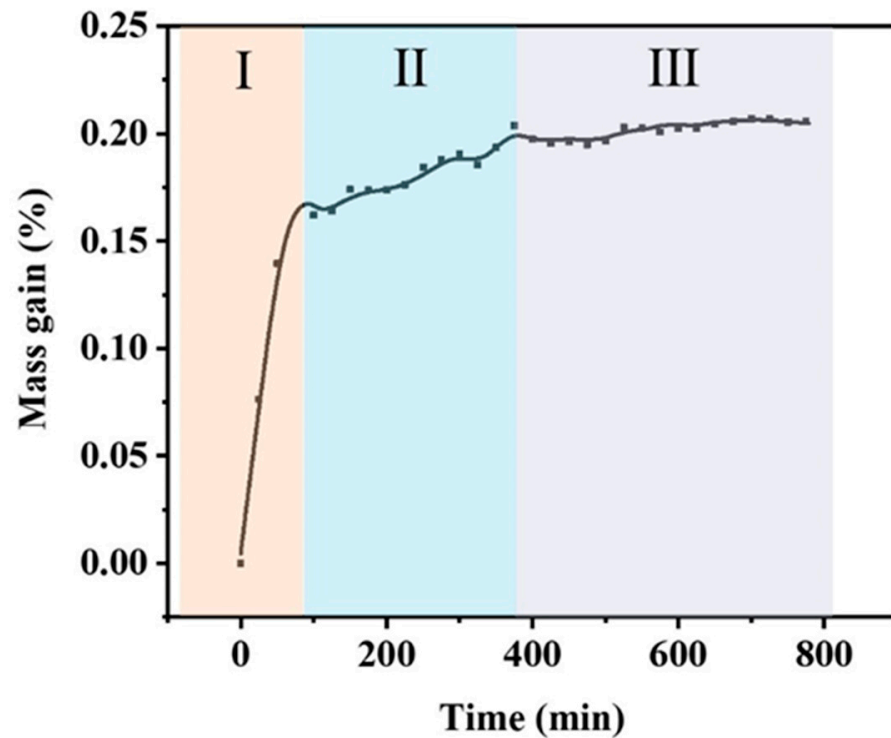


Figure 4. Isothermal oxidation curves of the coating.

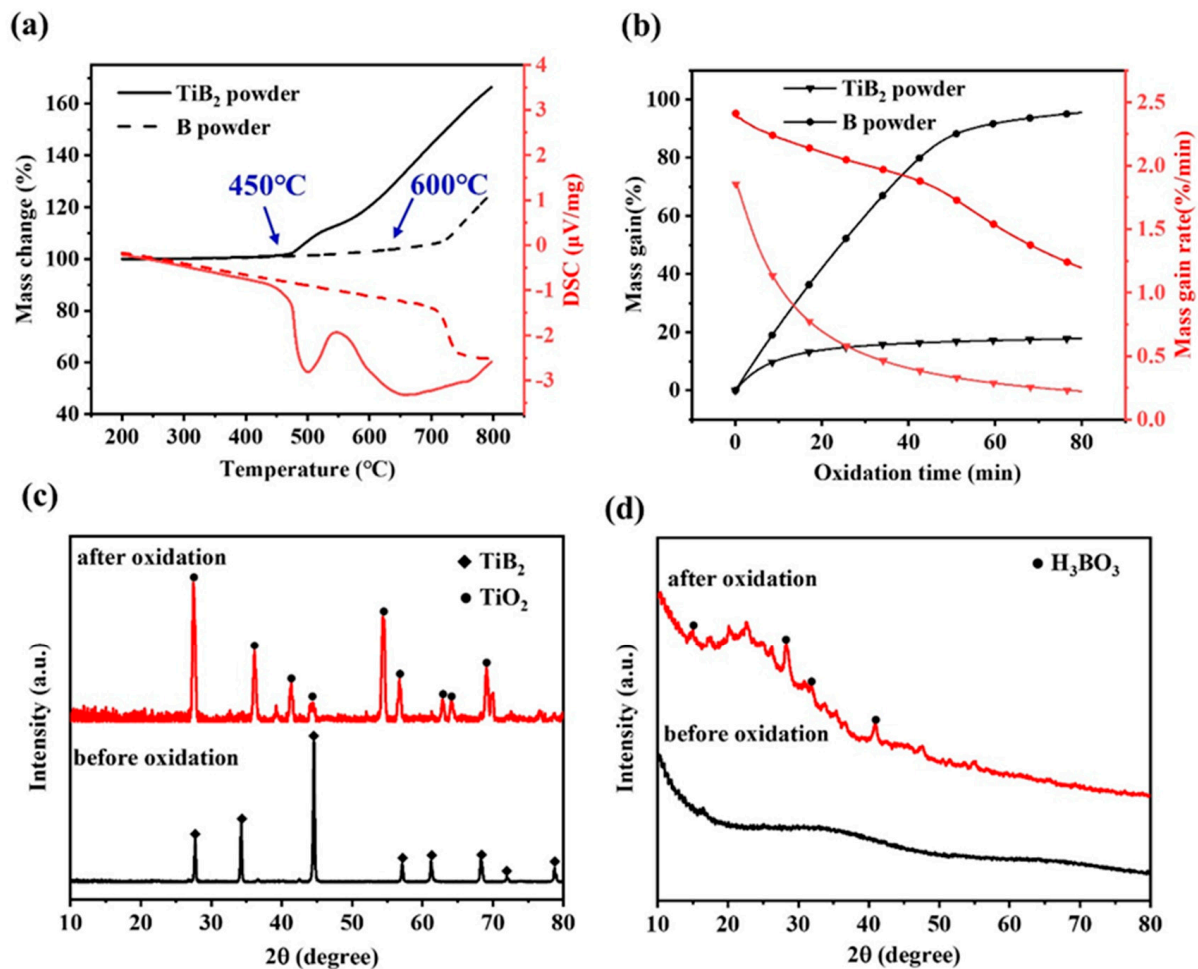
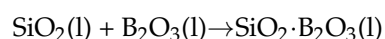
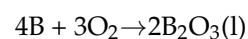
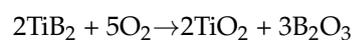


Figure 5. (a,b) TG–DSC and isothermal oxidation curves of TiB₂ and B powders, respectively; (c,d) XRD patterns of the TiB₂ and B powders after oxidation in 800 °C.

It is also found that the initial oxidation temperature of TiB₂ powder in Figure 5a is about 450 °C [31], which is significantly lower than that of B powder at 600 °C [32]. At the same time, the oxidation trend of TiB₂ in air is significantly greater than that of B. Therefore, the presence of B allows the coating to better form an oxide layer. At the same time, SiCN undergoes a high-temperature reaction, leading to the generation of SiO₂, which effectively repairs any cracks caused by oxidation. And the changes of substances before and after exposure to high temperatures of the thin-film coatings are analyzed using X-ray photoelectron spectroscopy (XPS). The full spectra (Figure 6a) reveal a noticeable increase in the concentration of O and B on the sample surface following exposure to high temperatures. The Si 2p spectrum (Figure 6b) demonstrates the presence of Si–O bonds (at 104.3 eV), indicating the formation of SiO₂. On the other hand, the analysis of the B 1s spectrum (Figure 6c) confirms the existence of solely B–O bonds after the high-temperature treatment. The possible oxidation reactions were shown as follows [33–35]



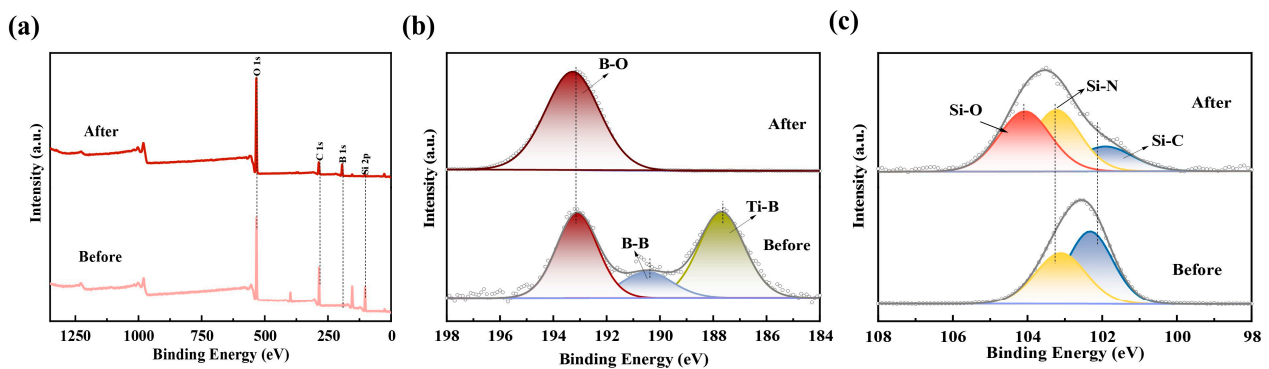


Figure 6. The sample surface before and after exposure to 800 °C (a) Full spectrum of XPS. (b) B 1s spectra and (c) Si 2p spectra before and after exposure to high temperature.

The phase transformation of the coating during the oxidation process was investigated by XRD analysis for different oxidation times (Figure 7). After 1 h of oxidation, SiO_2 , B_2O_3 and TiO_2 phases appeared. It showed that a glassy oxide layer was formed on the surface of the coating, and after 5 h, the peak strength of B_2O_3 (Figure 7) increased, indicating that the density of the antioxidant layer was also enhanced (Figure 8b,c). Figure 8 shows the evolution of surface and cross-sectional topography during oxidation of the coating. After oxidation at 800 °C for 1 h (Figure 8a), 5 h (Figure 8b), 10 h (Figure 8c), an oxide film is formed on its surface, which is dense and has no micropores. According to the specific gravity analysis of the elements of points EDS (Figure 8(a3,b3,c3)), the O content is higher, followed by the B content. Combined with the results of XRD (Figure 7), a dense $\text{B}_2\text{O}_3 \cdot \text{SiO}_2$ glass layer forms on the surface of the coating. At the same time, the cross-sectional topography of the coating is analyzed. After 1 h of oxidation (Figure 8(a1,a2)), the O element on the outside of the coating is higher than the inside, and the distribution of Ti elements is granular, indicating that the particles inside the coating are not completely oxidized. After 10 h of oxidation (Figure 8(b1,b2)), a dense oxide layer (thickness: $\sim 8 \mu\text{m}$) is formed on the surface of the coating, the surface of which is covered by a thick glass layer.

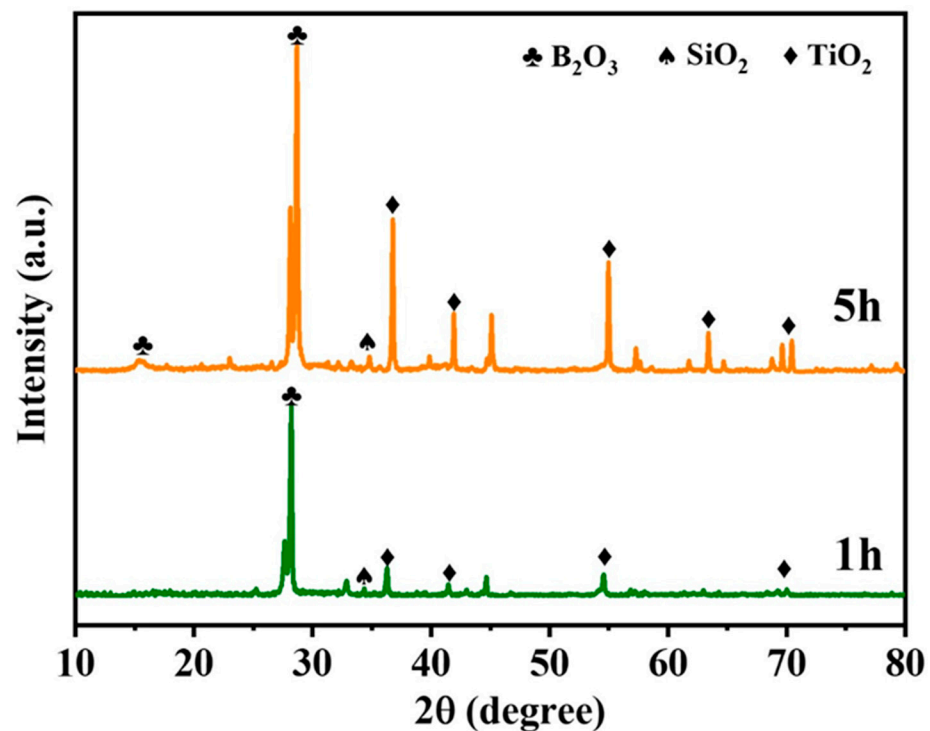


Figure 7. XRD patterns of the coating after oxidation for different times.

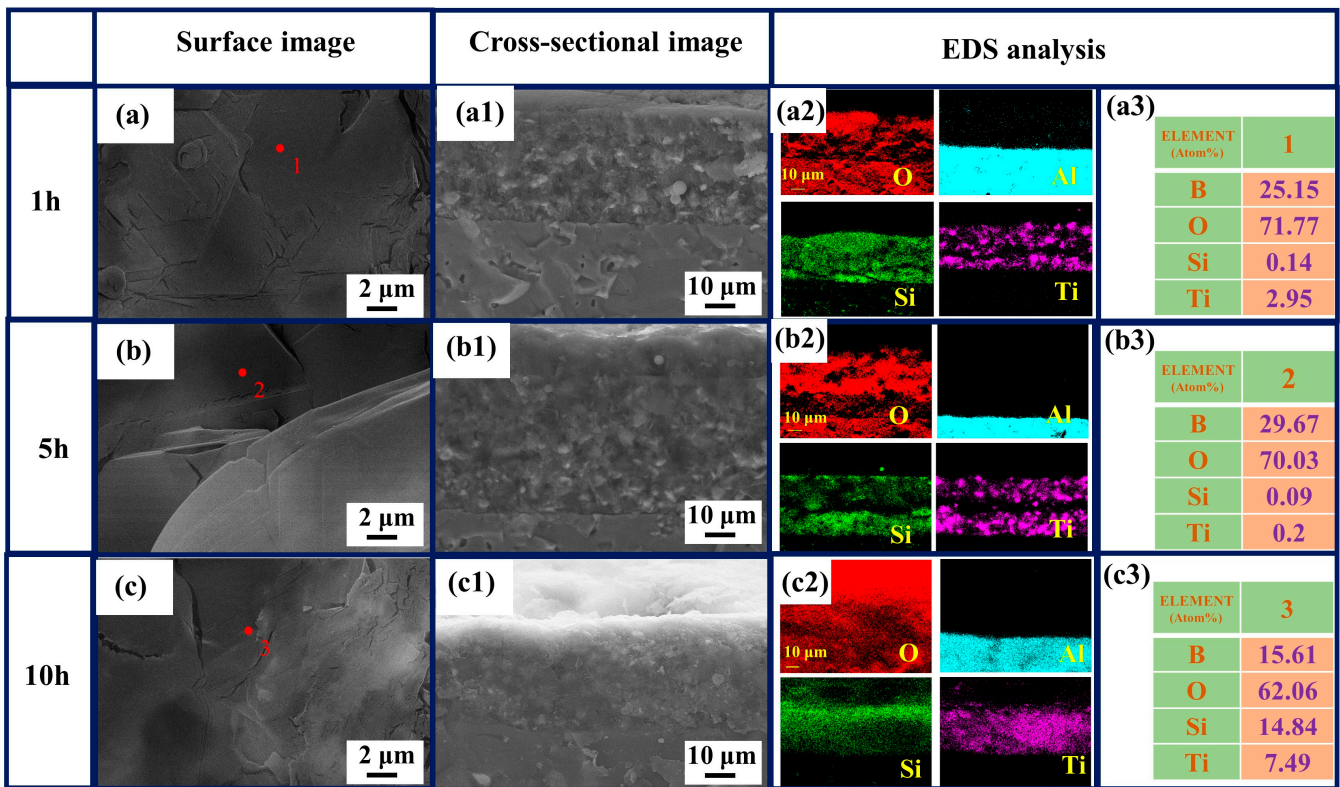


Figure 8. Surface and cross-sectional topography of the coating after oxidation for different times: 1 h (a–a3); 5 h (b–b3); 10 h (c–c3); element distribution map (a2,b2,c2) of the SEM image (a1,b1,c1); EDS analysis (a3,b3,c3) of spot 1, 2 and 3 (a,b,c).

3.3. Ablation Behavior of the Coated Samples at Different Times

To evaluate the protective performance of antioxidant films against erosion in high-velocity airflow environments, a flame spray apparatus was employed to assess their ablation resistance. Figure 9a illustrates the film's ablation process at a central temperature of 1000 °C and the thickness change of the ablation pit is calculated. Figure 9b presents the linear ablation rates of the film samples at different time intervals, revealing rates of 1.42 μm/min, 1.41 μm/min, and 1.04 μm/min at 4 min, 10 min, and 15 min, respectively. These results indicate a progressive reduction in film thickness and ablation rate as the duration of ablation increases. At the same time, the line ablation rate decreases with time.

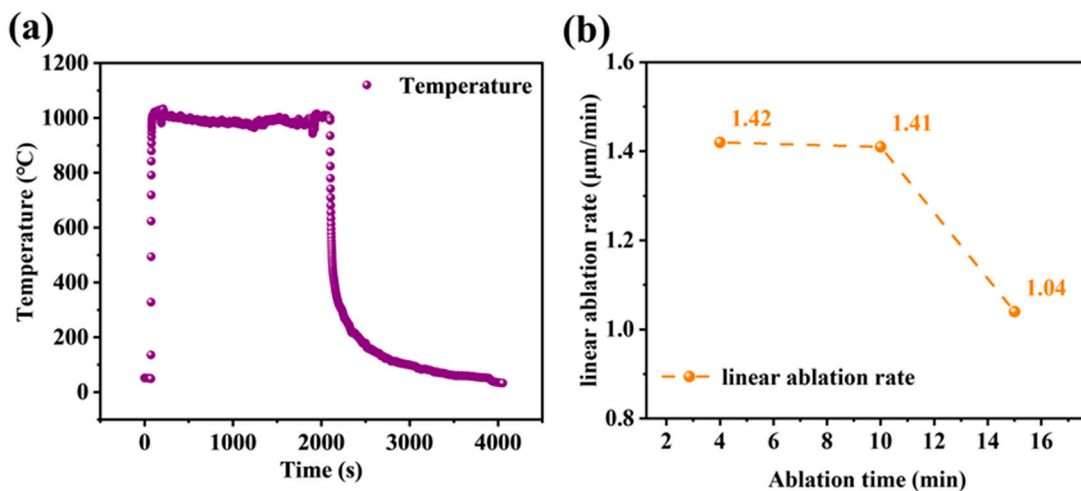


Figure 9. (a) Ablation center temperature curves; (b) Variations of linear ablation rates.

Figure 10 displays the XRD spectrum of the ablated film samples, demonstrating the presence of residual oxides primarily composed of B_2O_3 , TiO_2 , and SiO_2 on the surface. The oxide (B_2O_3 and SiO_2) appears on the sample surface according to XPS (Figure 11), although their content is relatively less than annealing completed. The Si-O bond content was 9.43% (Figure 11c), lower than 41.66% (Figure 6c). SEM images (Figure 12(a,a1)) reveal the film's intact morphology without visible voids or cracks after 4 min of ablation. However, after 10 min of ablation, surface melting occurs, exposing TiB_2 and TiO_2 particles (Figure 12(b1,b2)). The low melting point of B_2O_3 (450 °C) leads to the volatilization of the surface oxides under the high-temperature conditions of 1000 °C. After 30 min of ablation, distinct ablation pits appear on the surface, accompanied by a decrease in the proportion of B and Si as observed through EDS analysis (Figure 12(a1,b1,c1)). Despite the presence of surface voids, cross-sectional analysis (Figure 12c) confirms the film's adherence to the alumina substrate without detachment or oxidation fractures. This integrity is maintained even after 4 min (Figure 13a) and 10 min (Figure 13b) of ablation. After 30 min of ablation, a noticeable thinning of the cross-section (Figure 13c) is observed. During the ablation process, the possible oxidation reactions were shown as follows:

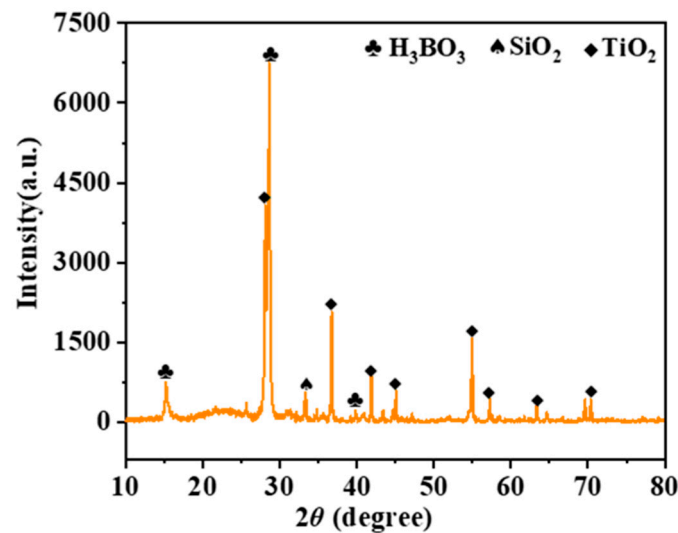


Figure 10. XRD patterns of the coating after ablation in flame.

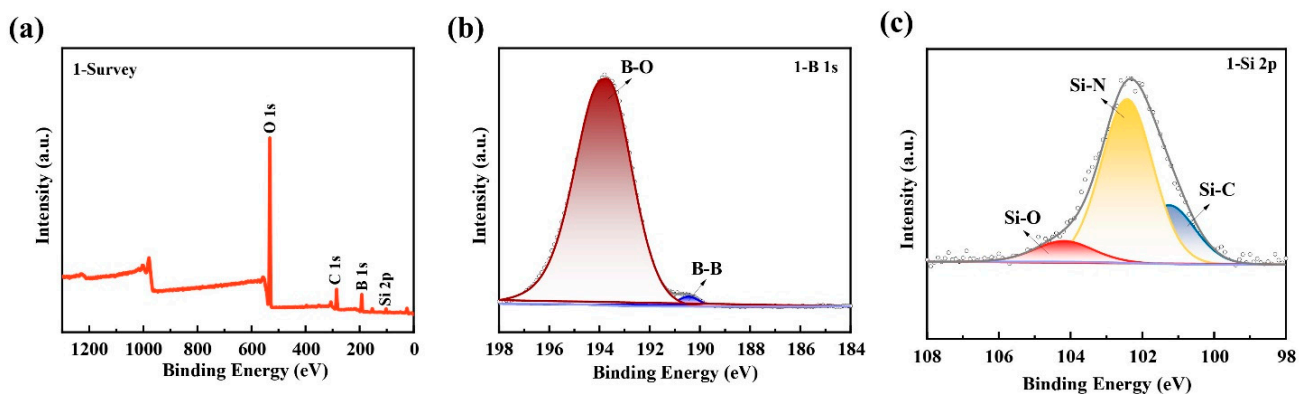


Figure 11. The sample surface after ablation (a) Full spectrum of XPS. (b) B 1s spectra and (c) Si 2p spectra before and after exposure to high temperature.

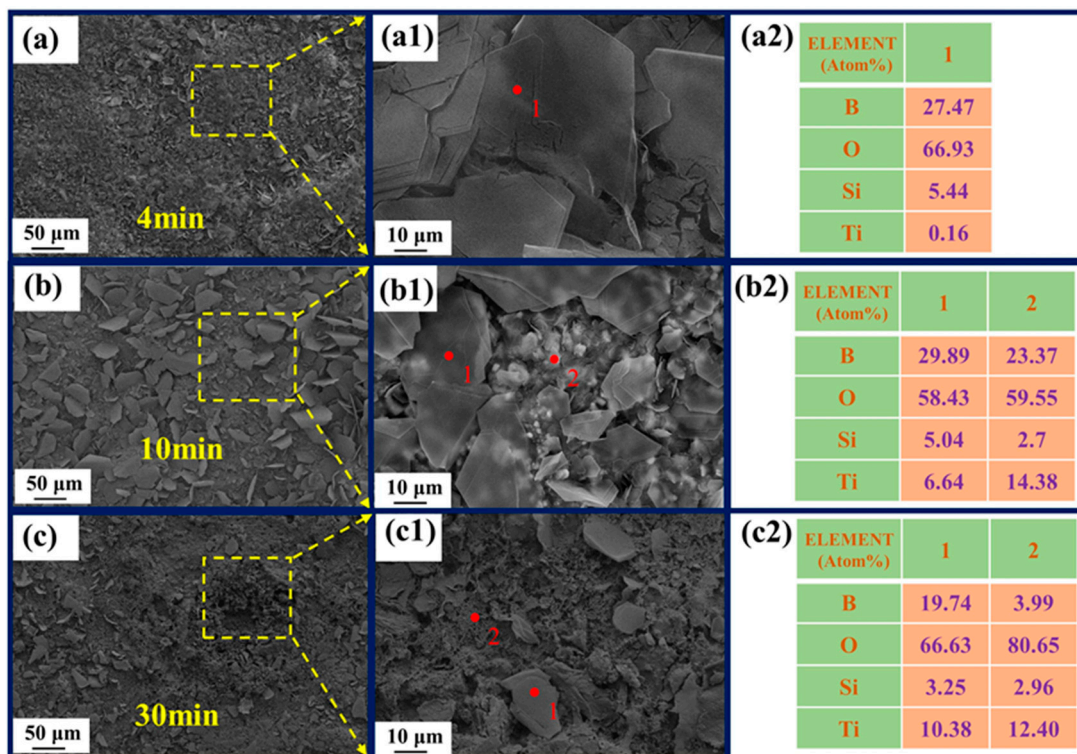


Figure 12. Surface SEM micrographs of different times: 4 min (a–a2); 10 min (b–b2); 30 min (c–c2); EDS analysis (a2,b2,c2) of spot 1, 2 (a1,b1,c1).

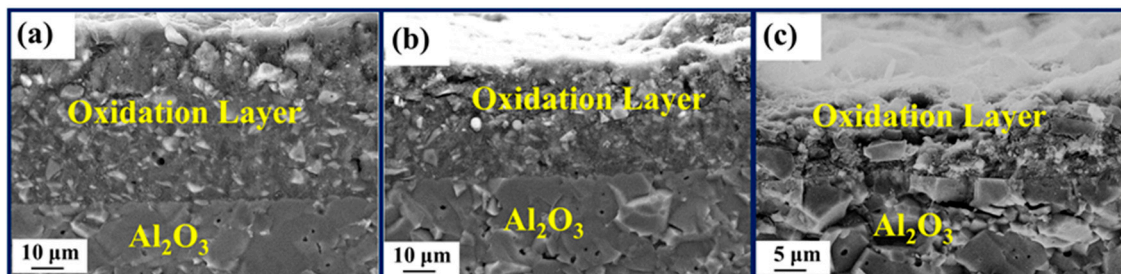


Figure 13. Cross-section SEM micrographs of different times: 4 min (a); 10 min (b); 30 min (c).

3.4. Thin-Film Temperature Sensor Oxidation Resistance Ablation Test

By fabricating the thin-film coating directly on the alumina substrate, the oxidation and ablation exploration of the thin-film coating was completed. Finally, we used the electrical resistance characteristics of thin-film sensors to characterize the performance of ablation process coating. The thin-film coating was applied to the sensitive layer as an antioxidation layer forming a double-layer structure [16]. Figure 14a illustrates the optical image of the sensor prior to ablation, displaying a predominantly light yellow surface. After 30 min of ablation, the surface exhibited a deep blue color without any signs of cracking or delamination. Analysis of the film sensor's resistance variation demonstrated its impressive antioxidation performance even at the elevated temperature of 1000 °C (Figure 14b). Upon undergoing pyrolysis [15] at 1000 °C, the film sensor experienced a decrease in resistance, ultimately reaching a stable state with a rate of change of 1.88% over 25 min (Figure 14c). After the ablation process is completed, the resistance of the thin-film sensor can be restored to its initial value. The cross-sectional image after 30 min ablation of the sensor is shown in Figure 15a. The antioxidant layer remains firmly bonded to the sensitive layer without any cracks, despite the destruction of the protective glass layer formed on the surface of the film. In addition, the EDS analysis of the sensor cross-section (Figure 15b) shows a decrease

in Si content above the antioxidant layer and the presence of a large amount of Si elements in the middle. Meanwhile, the Ti elements in the cross-section are uniformly distributed. During the ablation process, the vaporization of B_2O_3 decreased the surface temperature. Since SiO_2 loses its stability above $2300\text{ }^\circ\text{C}$ due to rapid evaporation [36,37], at $1000\text{ }^\circ\text{C}$, high viscosity SiO_2 flows with the ablation gas stream and it is difficult to evaporate, and liquid SiO_2 forms a dense layer on the ablation surface. By introducing Ti (TiB_2), the film did not exfoliate significantly and the impact resistance of the film was enhanced.

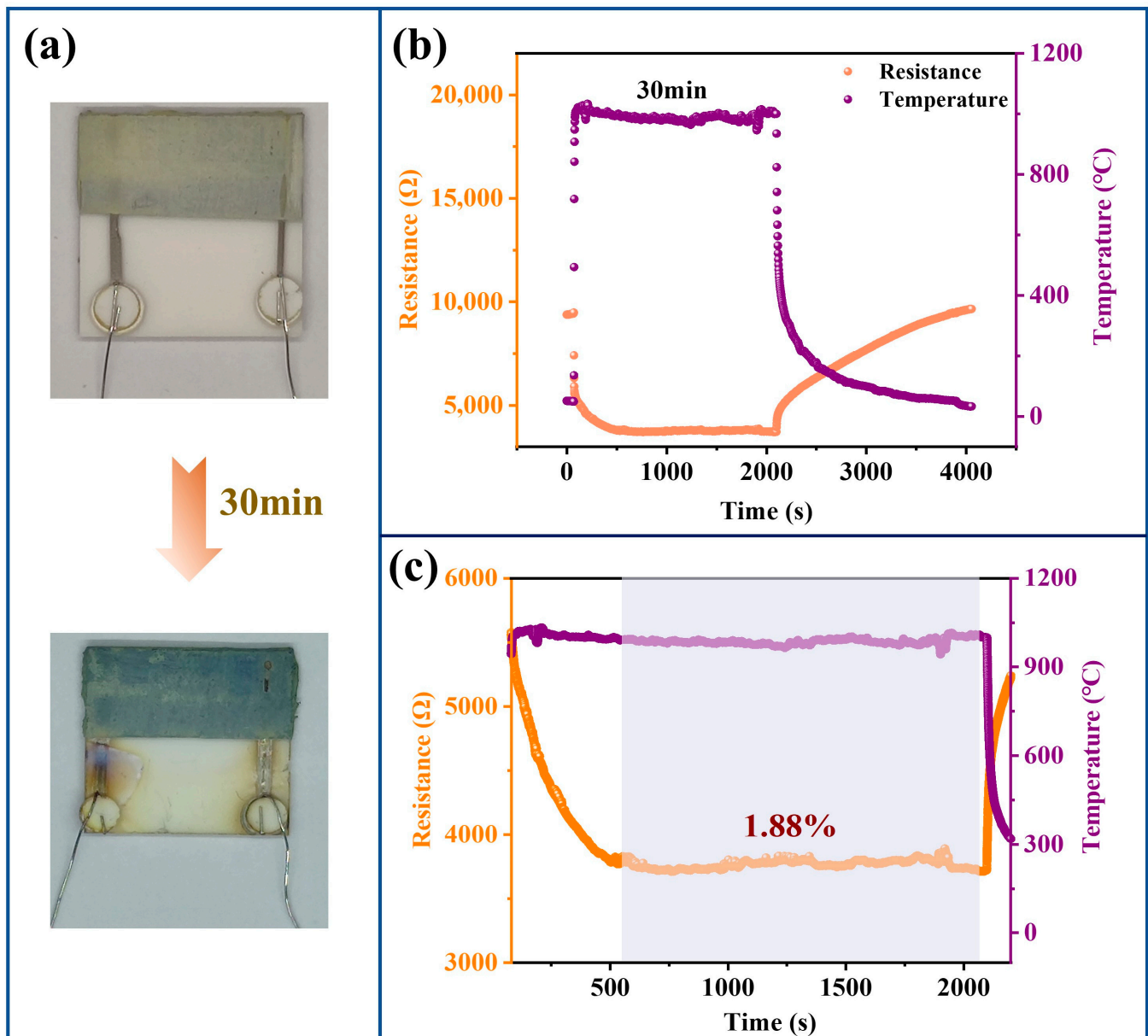


Figure 14. (a) Pre- and post-ablation film sensor; (b) Resistance variation of the film sensor during the ablation process; (c) Magnified view of (b).

To gain a comprehensive understanding of the oxidation and ablation resistance mechanism of the PDC/ TiB_2 /B composite film, Figure 16 illustrates a simplified schematic. The thin-film coating is applied onto a sensitive layer that undergoes rapid oxidation and converts to Si, Ti, and B oxides at elevated temperatures. A highly viscous and fluid SiO_2 - B_2O_3 glass layer is swiftly formed, effectively blocking the infiltration of oxygen. During the ablation process, the film surface temperature rises rapidly, leading to the volatilization of B_2O_3 , which results in the formation of ablation products, such as SiO_2

and borosilicate, which are carried by the ablation airflow within and around the coating. While SiO_2 exhibits low evaporation at $1000\text{ }^\circ\text{C}$, it remains deposited on the film surface, forming a high-viscosity SiO_2 layer. This layer restricts the ingress of oxidizing gases into the film coating, thereby preventing further oxidation.

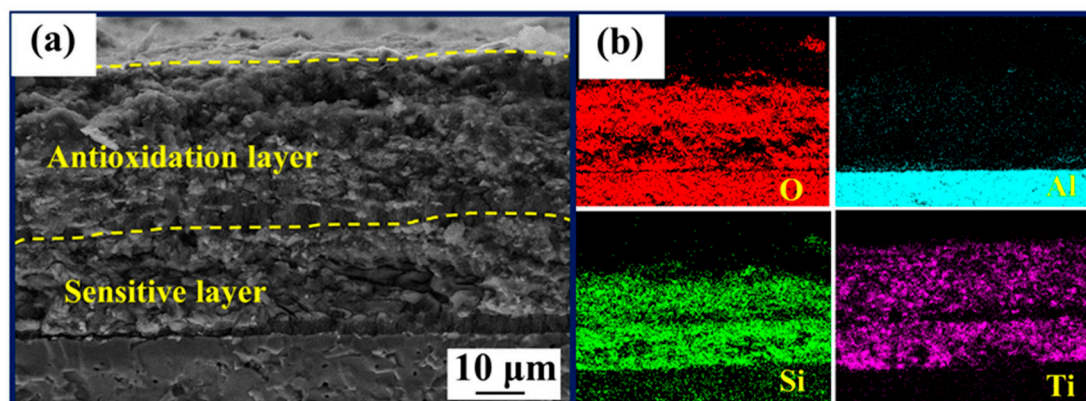


Figure 15. (a) Cross-sectional view of the film sensor after ablation; (b) EDS analysis of the cross-section.

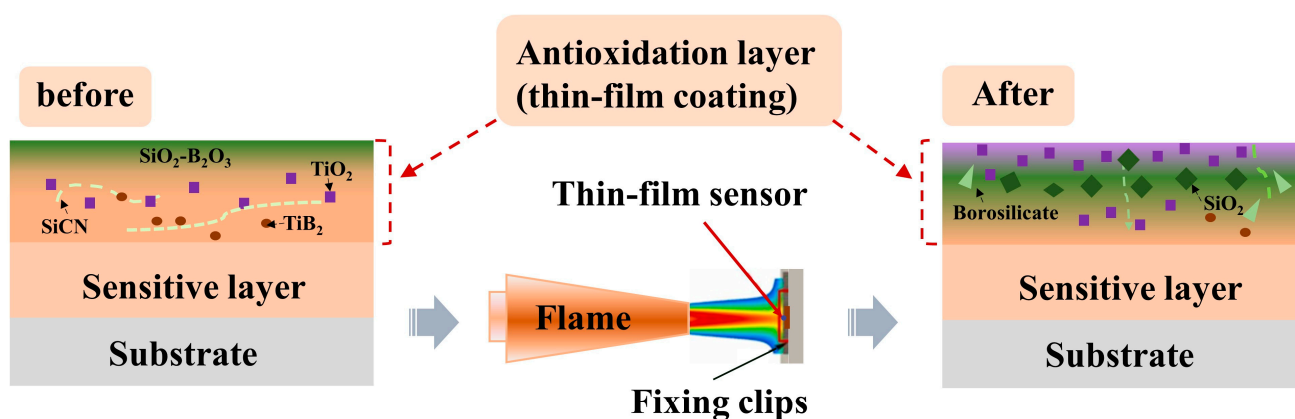


Figure 16. Schematic diagram illustrating the anti-ablation of the thin-film coatings.

4. Conclusions

This study focuses on investigating the oxidation and ablation behavior of PDC/ TiB_2 /B composites, which has an enhancing effect on the performance of PDC thin-film sensors. Through high-temperature heat treatment, a dense $\text{SiO}_2\text{-B}_2\text{O}_3$ oxide layer forms on the surface of the thin-film coating, effectively preventing further oxidation of the sensitive layer by oxygen. After oxidation in air at $800\text{ }^\circ\text{C}$ for 10 h, the sample experiences only a 0.2% mass loss. Moreover, the generated oxide layer is also critical to the improvement of the ablation resistance. During high-temperature ablation at $1000\text{ }^\circ\text{C}$, the B_2O_3 on the coating's surface absorbs and dissipates heat, leading to its significant volatilization. Simultaneously, the SiCN ceramic absorbs heat and undergoes further oxidation, resulting in the formation of new SiO_2 . This process replenishes the vaporized B_2O_3 and contributes to the enhanced ablation resistance of the coating. After being exposed to the butane flame for 15 min, the coating demonstrates remarkable resistance to ablation, with a linear ablation rate of $1.04\ \mu\text{m}/\text{min}$. And the thin-film sensor exhibits an impressive resistance change rate of $0.0752\%/ \text{min}$ at $1000\text{ }^\circ\text{C}$. Consequently, the particle-filled PDC composite film coating has a key role in improving the oxidation and ablation performance of thin-film sensors. This work also provides insights and guidance for the design and development of thin-film coatings in extreme environments with high application potential.

Author Contributions: L.L.: conceptualization, methodology, formal analysis, investigation, data curation, visualization, writing—original draft, review, and editing. Y.H.: methodology, data curation, and visualization. L.X.: review, editing, and supervision. C.S.: review, editing, and supervision. G.H.: conceptualization, methodology, review, editing, and supervision. D.S. and Z.H.: conceptualization, methodology, review, editing, and supervision. All authors have read and agreed to the published version of the manuscript.

Funding: This research was supported by the National Key R & D Program of China 2021YFB3200701 and the National Natural Science Foundation of China (Grant No. 62101469).

Institutional Review Board Statement: Not applicable.

Informed Consent Statement: Not applicable.

Data Availability Statement: The data presented in this study are available on request from the corresponding author.

Conflicts of Interest: The authors declare no conflict of interest.

References

1. Yang, S.Y.; Li, H.F.; Lin, X.K.; Yao, J.Y.; Yang, Z.Q.; Zhang, C.C.; Wang, H.; Ding, G.F. Effect of Al₂O₃/Al bilayer protective coatings on the high-temperature stability of PdCr thin film strain gages. *J. Alloys Compd.* **2018**, *759*, 1–7. [[CrossRef](#)]
2. Wrbanek, J.; Fralick, G.; Gonzalez, J. Developing multilayer thin film strain sensors with high thermal stability. In Proceedings of the 42nd AIAA/ASME/SAE/ASEE Joint Propulsion Conference & Exhibit, Sacramento, CA, USA, 9–12 July 2006.
3. Liu, H.; Mao, X.L.; Yang, Z.B.; Cui, J.T.; Jiang, S.W.; Zhang, W.L. High temperature static and dynamic strain response of PdCr thin film strain gauge prepared on Ni-based superalloy. *Sens. Actuator A-Phys.* **2019**, *298*, 9. [[CrossRef](#)]
4. Wen, Q.B.; Yu, Z.J.; Riedel, R. The fate and role of in situ formed carbon in polymer-derived ceramics. *Prog. Mater. Sci.* **2020**, *109*, 63. [[CrossRef](#)]
5. Cao, Y.J.; Yang, X.P.; Zhao, R.; Chen, Y.H.; Li, N.; An, L.N. Giant piezoresistivity in polymer-derived amorphous SiAlCO ceramics. *J. Mater. Sci.* **2016**, *51*, 5646–5650. [[CrossRef](#)]
6. Shao, G.; Jiang, J.; Jiang, M.; Su, J.; Liu, W.; Wang, H.; Xu, H.; Lit, H.; Zhang, R. Polymer-derived SiBCN ceramic pressure sensor with excellent sensing performance. *J. Adv. Ceram.* **2020**, *9*, 374–379. [[CrossRef](#)]
7. Ma, B.S.; Wang, Y.G. Fabrication of dense polymer-derived silicon carbonitride ceramic bulks by precursor infiltration and pyrolysis processes without losing piezoresistivity. *J. Am. Ceram. Soc.* **2018**, *101*, 2752–2759. [[CrossRef](#)]
8. Wu, C.; Pan, X.C.; Lin, F.; Cui, Z.F.; He, Y.P.; Chen, G.C.; Zeng, Y.J.; Liu, X.L.; Chen, Q.N.; Sun, D.H.; et al. TiB₂/SiCN Thin-Film Strain Gauges Fabricated by Direct Writing for High-Temperature Application. *IEEE Sens. J.* **2022**, *22*, 11517–11525. [[CrossRef](#)]
9. Wu, C.; Pan, X.C.; Lin, F.; Cui, Z.F.; Li, X.; Chen, G.C.; Liu, X.L.; He, Y.P.; He, G.H.; Hai, Z.Y.; et al. High-temperature electrical properties of polymer-derived ceramic SiBCN thin films fabricated by direct writing. *Ceram. Int.* **2022**, *48*, 15293–15302. [[CrossRef](#)]
10. Jung, S.; Seo, D.; Lombardo, S.J.; Feng, Z.C.; Chen, J.K.; Zhang, Y.W. Fabrication using filler controlled pyrolysis and characterization of polysilazane PDC RTD arrays on quartz wafers. *Sens. Actuator A-Phys.* **2012**, *175*, 53–59. [[CrossRef](#)]
11. Seo, D.; Jung, S.H.; Lombardo, S.J.; Feng, Z.C.; Chen, J.K.; Zhang, Y.W. Fabrication and electrical properties of polymer-derived ceramic (PDC) thin films for high-temperature heat flux sensors. *Sens. Actuator A-Phys.* **2011**, *165*, 250–255. [[CrossRef](#)]
12. Ma, B.S.; Cao, Y.J.; Gao, Y.; Wang, Y.G. Fabrication of a thin double-layer thermistor based on DVB-modified polymer-derived SiCN ceramics. *J. Alloys Compd.* **2018**, *732*, 491–497. [[CrossRef](#)]
13. Li, L.; Xu, L.; He, Y.; Chen, G.; Zeng, Y.; Shao, C.; He, L.T.G.; Zhao, Y.; Sun, D.; Hai, Z.J.I.S.J. Fabrication of High-temperature Polymer-Derived Ceramic Thin Film Heat Flux Sensor by 3D Printing and Laser Pyrolysis. *IEEE Sens. J.* **2023**, *23*, 15391–15399. [[CrossRef](#)]
14. Cui, Z.F.; Li, X.; Chen, G.C.; Wu, C.; He, G.H.; Hai, Z.Y.; Chen, Q.N.; Sun, D.H. Thin-film temperature sensor made from particle-filled polymer-derived ceramics pyrolyzed in vacuum. *J. Eur. Ceram. Soc.* **2022**, *42*, 2735–2742. [[CrossRef](#)]
15. Cui, Z.F.; Chen, G.C.; Li, X.; Wu, C.; He, G.H.; Hai, Z.Y.; Chen, Q.N.; Sun, D.H. An anti-oxidative coating made from particle-filled SiCN precursor for applications up to 800 degrees C. *J. Alloys Compd.* **2022**, *913*, 7. [[CrossRef](#)]
16. Xu, L.; Li, L.; Tang, L.; Zeng, Y.; Chen, G.; Shao, C.; Wu, C.; He, G.; Chen, Q.; Fang, G.; et al. Rapid Printing of High-Temperature Polymer-Derived Ceramic Composite Thin-Film Thermistor with Laser Pyrolysis. *ACS Appl. Mater. Interfaces* **2023**, *15*, 9996–10005. [[CrossRef](#)]
17. Wu, C.; Pan, X.C.; Lin, F.; Chen, G.C.; Xu, L.D.; Zeng, Y.J.; He, Y.P.; Sun, D.H.; Hai, Z.Y. Al₂O₃-Modified Polymer-Derived Ceramic SiCN High-Temperature Anti-Oxidative Composite Coating Fabricated by Direct Writing. *Polymers* **2022**, *14*, 11. [[CrossRef](#)]
18. Zhang, J.P.; Qu, J.L.; Fu, Q.G. Ablation behavior of nose-shaped HfB₂-SiC modified carbon/carbon composites exposed to oxyacetylene torch. *Corros. Sci.* **2019**, *151*, 87–96. [[CrossRef](#)]
19. Vinci, A.; Zoli, L.; Landi, E.; Sciti, D. Oxidation behaviour of a continuous carbon fibre reinforced ZrB₂-SiC composite. *Corros. Sci.* **2017**, *123*, 129–138. [[CrossRef](#)]

20. Jiang, Y.; Yin, S.; Li, M.F.; Zhang, Z.Q.; Tang, G.L.; Wang, N.; Ru, H.Q. Oxidation and ablation behaviour of multiphase ultra-high-temperature ceramic Ta_{0.5}Zr_{0.5}B₂-Si-SiC protective coating for graphite. *Ceram. Int.* **2021**, *47*, 11358–11371. [[CrossRef](#)]
21. Kong, J.A.; Zhang, Y.L.; Wang, H.H.; Chen, G.H.; Gai, W.H.; Zhang, P.F.; Li, H.J. Sublayer design and ablation resistance of CVD-TaC alternate coatings with different crystallite morphologies for C/C composites. *J. Mater. Sci. Technol.* **2023**, *141*, 1–10. [[CrossRef](#)]
22. Liu, T.Y.; Fu, Q.G.; Zhang, J.P. Microstructure and mechanical performance evolution of C/C-ZrC composites exposed to oxyacetylene flame. *Ceram. Int.* **2021**, *47*, 22654–22661. [[CrossRef](#)]
23. Liao, N.; Jia, D.C.; Yang, Z.H.; Niu, B.; Zhou, Y.; Li, Y.W. Enhanced mechanical properties, thermal shock resistance and ablation resistance of Si₂BC₃N ceramics with nano ZrB₂ addition. *J. Eur. Ceram. Soc.* **2019**, *39*, 846–859. [[CrossRef](#)]
24. Wang, Y.; Chen, Z.F.; Yu, S.J. Ablation behavior and mechanism analysis of C/SiC composites. *J. Mater. Res. Technol.-JMRT* **2016**, *5*, 170–182. [[CrossRef](#)]
25. Turcer, L.R.; Pature, N.P. Towards multifunctional thermal environmental barrier coatings (TEBCs) based on rare-earth pyrosilicate solid-solution ceramics. *Scr. Mater.* **2018**, *154*, 111–117. [[CrossRef](#)]
26. Zhu, X.F.; Zhang, Y.L.; Li, H.G.; Zhang, J.; Fu, Y.Q.; Su, Y.Y. SiC/SiC-ZrSi₂ coating with micro-pore to protect C/C composites against oxidation for long-life service at high temperatures. *Corrosion Sci.* **2021**, *191*, 11. [[CrossRef](#)]
27. Hayashi, H.; Watanabe, M.; Inaba, H. Measurement of thermal expansion coefficient of LaCrO₃. *Thermochim. Acta* **2000**, *359*, 77–85. [[CrossRef](#)]
28. Munro, R.G. Material Properties of Titanium Diboride. *J. Res. Natl. Inst. Stand. Technol.* **2000**, *105*, 709–720. [[CrossRef](#)]
29. Lundström, T.; Lönnberg, B.; Bauer, J. Thermal expansion of β rhombohedral boron. *J. Alloys Compd.* **1998**, *267*, 54–58. [[CrossRef](#)]
30. Schultes, G.; Schmitt, M.; Goettel, D.; Freitag-Weber, O. Strain sensitivity of TiB₂, TiSi₂, TaSi₂ and WSi₂ thin films as possible candidates for high temperature strain gauges. *Sens. Actuator A-Phys.* **2006**, *126*, 287–291. [[CrossRef](#)]
31. Kohn, J.A.; Nye, W.F.; Gaulé, G.K. *Boron Synthesis, Structure, and Properties: Proceedings of the Conference on Boron*; Springer: Berlin/Heidelberg, Germany, 2013.
32. Kulpa, A.; Troczynski, T. Oxidation of TiB₂ powders below 900 degrees C. *J. Am. Ceram. Soc.* **1996**, *79*, 518–520. [[CrossRef](#)]
33. Ivashchenko, V.I.; Kozak, A.O.; Porada, O.K.; Ivashchenko, L.A.; Sinelnichenko, O.K.; Lytvyn, O.S.; Tomila, T.V.; Malakhov, V.J. Characterization of SiCN thin films: Experimental and theoretical investigations. *Thin Solid Film.* **2014**, *569*, 57–63. [[CrossRef](#)]
34. Senda, T. Oxidation behavior of titanium boride at elevated temperatures. *J. Ceram. Soc. Jpn* **1996**, *104*, 785–787. [[CrossRef](#)]
35. Jain, A.; Anthonysamy, S. Oxidation of boron carbide powder. *J. Therm. Anal. Calorim.* **2015**, *122*, 645–652. [[CrossRef](#)]
36. Zhang, C.; Zhang, Y.; Zhao, D.; Hu, H.; Zhang, Z. Mechanism of ablation of 3D C/ZrC-SiC composite under an oxyacetylene flame. *Corros. Sci.* **2013**, *68*, 168–175.
37. Li, Z.; Li, H.; Zhang, S.; Wang, J.; Li, W.; Sun, F. Effect of reaction melt infiltration temperature on the ablation properties of 2D C/C-SiC-ZrC composites. *Corros. Sci.* **2012**, *58*, 12–19. [[CrossRef](#)]

Disclaimer/Publisher's Note: The statements, opinions and data contained in all publications are solely those of the individual author(s) and contributor(s) and not of MDPI and/or the editor(s). MDPI and/or the editor(s) disclaim responsibility for any injury to people or property resulting from any ideas, methods, instructions or products referred to in the content.